coatings

Article

The Corrosion Resistance of Concrete-Filled Steel Tubes with the Assembly Unit of Na_2MoO_4 and Benzotriazole

Di Wang [1], Zhiqiang Xu [1], Na Xu [1], Zengliang Hu [1], Hui Wang [2,*] and Feiting Shi [2]

[1] School of Chemical Engineering and Machinery, Liaodong University, Dandong 118000, China; xuna@elnu.edu.cn (N.X.); huzengliang@elnu.edu.cn (Z.H.)
[2] School of Civil Engineering and Geographic Environment, Ningbo University, Ningbo 315000, China
* Correspondence: huiwang123@aliyun.com

Abstract: Steel pipes are commonly used to strengthen the concrete's load-bearing capacity. However, they are prone to corrosion in salt erosion environments. In this study, the influence of Na_2MoO_4 and benzotriazole on concrete-filled steel tubes' corrosion performance is investigated. The steel pipes' mass loss rates (MRs), ultrasonic velocity, electrical resistance, and the AC impedance spectrum and Tafel curves of concrete-filled steel tubes were used to characterize the degree of corrosion in the steel pipes. Scanning electron microscopy–energy-dispersive spectrometry and X-ray diffraction were used for studying the composition of steel pipe rust. The research results revealed that the NaCl freeze–thaw cycles (F-C) and NaCl dry–wet alternation (D-A) actions had a reducing effect on the mass and ultrasonic velocity of the concrete-filled steel tubes. After 300 NaCl F-C and 30 NaCl D-A, the MRs were 0%~0.00470% and 0%~0.00666%. The corresponding ultrasonic velocities were 0%~21.1% and 0%~23.6%. When a rust inhibitor was added, the results were the opposite. The MRs decreased by 0%~80.3% and 0%~81.6% with the added Na_2MoO_4 and benzotriazole. Meanwhile, the corresponding ultrasonic velocities were 0%~8.1% and 0%~8.3%. The steel tubes were corroded after 300 NaCl F-C and 30 NaCl D-A. The addition of rust inhibitors improved the corrosion resistance of the concrete-filled steel tubes by increasing the electrical resistance before NaCl erosion. The corrosion area rate decreased by using the rust inhibitors. The corrosion resistance effect of benzotriazole was higher than that of Na_2MoO_4. The concrete-filled steel tube with an assembly unit comprising 5 kg/m^3 of Na_2MoO_4 and 15 kg/m^3 of benzotriazole had the best corrosion resistance under the erosion induced by NaCl F-C and D-A. Rust inhibitors reduced the content of iron-containing crystals and iron elements. The specimens with 5 kg/m^3 Na_2MoO_4 and 15 kg/m^3 benzotriazole had the lowest concentration of iron-containing crystals and iron elements.

Keywords: steel pipes; corrosion resistance; inhibitors; AC impedance spectrum; Tafel curves

Citation: Wang, D.; Xu, Z.; Xu, N.; Hu, Z.; Wang, H.; Shi, F. The Corrosion Resistance of Concrete-Filled Steel Tubes with the Assembly Unit of Na_2MoO_4 and Benzotriazole. *Coatings* **2024**, *14*, 349. https://doi.org/10.3390/coatings14030349

Academic Editor: Jose Luis Viesca

Received: 13 February 2024
Revised: 7 March 2024
Accepted: 8 March 2024
Published: 14 March 2024

1. Introduction

Cement concrete is a kind of material widely applied in bridge and road engineering [1]. Steel bars, steel fibers, plant fibers, etc., are often used to enhance the strength and durability of concrete [2–4]. Zhang et al. [5,6] stated that steel fibers increased flexural and compressive strengths by 0%~48.2% and 0%~41.6%. Additionally, the impact toughness improved using polyethylene fibers, polyvinyl alcohol fibers, and steel fibers at increasing rates of 23.6%, 31.5%, and 41.7% respectively. Besides these methods for enhancing the performance of concrete, steel pipe confinement is also a commonly used method for improving the performance of concrete [7].

Steel tube-reinforced concrete is a type of concrete that fully combines the advantages of steel and concrete. This combination structure shows high bearing capacity, plasticity, convenient construction, toughness, and low cost. This type of structure has been widely used in construction and transportation engineering recently [8–11].

Dai revealed that steel tube-reinforced concrete exhibits good elastic–plastic and ductility performance [12]. Additionally, steel tube-reinforced concrete columns' ultimate bearing capacity increased by 73.6–112.1% compared to ordinary concrete columns. Zhong et al. reported that the creep coefficient of steel tube-reinforced concrete with a steel content of 13% was reduced by about 35% compared to steel tube concrete with a steel content of 4% [13,14]. George et al. indicated that steel tubes are effective in improving the durability of cement concrete [15]. The mechanical strength of steel tube-reinforced concrete did not decrease after long-term immersion in NaCl.

Concrete-filled steel pipes are prone to corrosion due to salt erosion, when this concrete is used in coastal environments. Corrosion easily occurs at the interface between steel pipes and concrete [16–20]. Although 316 L stainless steel with strong corrosion resistance can be used for steel pipe production, its high cost makes it difficult to use in practice [21]. Adding rust inhibitors to concrete is a good method for preventing steel pipe corrosion. Rust inhibitors can be divided into cathodic rust inhibitors and anodic rust inhibitors. Cathodic rust inhibitors can prevent steel from corrosion by forming an adsorption film on the steel. Meanwhile, the corrosion resistance of steel pipes is increased by anodic rust inhibitors due to the improved passivation film. The application of an assembly unit of cathodic and anodic rust inhibitors to enhance the corrosion resistance of concrete-filled steel tubes combines the advantages of these two kinds of rust inhibitors.

In this study, the corrosion resistance of concrete-filled steel tubes was investigated. The mass loss rates of steel tubes and the concrete-filled steel tubes' electrical parameters, including electrical resistance, as well as the values for the AC impedance spectra and Tafel curves, were obtained, which reflected the corrosion. The scanning electron microscopy images and X-ray diffraction curves of the rust on the surface of the steel tubes were generated to determine the corresponding corrosion. This research will provide a reference for improving the corrosion resistance of steel pipes used for concrete reinforcement.

2. Materials and Experimental Methods

2.1. Raw Materials

The ordinary Portland cement (OPC) offered by Jinhua Kunbang Decoration Materials Co., Ltd., Jinhua, China, was used as a binding material. Three types of materials were used, with densities of 3.21 g/cm^3, 2.93 g/cm^3, and 2.24 g/cm^3. OPC has an initial setting time of 113.4 min initial setting time and a final setting time of 246.7 min. Crushed granite gravel with a maximum particle diameter of 26.5 mm, a minimum diameter of 9.5 mm (continuous particle sizes), and a crushed index of 4.9% was used for coarse aggregates. River sand by Lingshou County Bo Vanadium Mineral Products Co., Ltd., Shijiazhuang, China, was used for fine aggregates, with a fineness modulus of 2.86. An efficient polycarboxylic acid water-reducing agent with a reducing rate of 40% was used for adjusting the fluidity of fresh cement concrete. Benzotriazole and sodium molybdate were provided by the Nanjing Milan New Materials Co., Ltd., Nanjing, China, and they were used as anodic and cathodic rust inhibitors, respectively. The corresponding pureness rates are 99.7% and 99.8%, respectively. Q355B steel pipes manufactured by Tianjin Baolai Steel Co., Ltd., Tianjin, China, were used in this research. The inside and outside diameters of the steel pipes were 100 mm and 80 mm, respectively. The properties of the cement and the corrosion inhibitors are shown in Tables 1 and 2 respectively.

Table 1. The properties of the cement.

Chemical Composition (%)								Loss on Ignition (%)	Median Diameter D_{50} (μm)
CaO	SiO_2	Al_2O_3	Fe_2O_3	MgO	MnO	R_2O	SO_3		
62.51	21.18	5.19	3.84	1.81	0.15	0.47	2.90	1.55	18.6

Table 2. The properties of the corrosion inhibitors.

Types	$Na_2MoO_4 \cdot 2H_2O$	Benzotriazole	Cl
Benzotriazole	/	99.6%	<0.02
Sodium olybdate	99.7%	/	<0.02

2.2. The Manufacturing Methods

Cement concrete was manufactured as follows: Firstly, aggregates were poured into an HJW-60 concrete single horizontal shaft-forced mixer and stirred at a mixing speed of 45 rpm per minute for 1 min. Then, cement was added, and the mixture was stirred for another 1 min. Ultimately, a mixture of water and water-reducing agent was added to the mixer, and the mixture was stirred at a rate of 45 rpm/min for 2 min, yielding fresh concrete. Table 3 shows the mixing proportions of the cement concrete used in the concrete-filled steel tubes.

Table 3. The mixing proportions of cement concrete used in the concrete-filled steel tubes.

Types	Water (kg)	Cement (kg)	Sand (kg)	Gravel (kg)	Na_2MoO_4 (kg)	Benzotriazole (kg)	WR (kg)
A_1	200.25	501.25	648.50	972.95	5	0	1
A_2	200.25	501.25	648.50	972.95	10	0	1
A_3	200.25	501.25	648.50	972.95	15	0	1
A_4	200.25	501.25	648.50	972.95	20	0	1
A_5	200.25	501.25	648.50	972.95	25	0	1
A_6	200.25	501.25	648.50	972.95	0	5	1
A_7	200.25	501.25	648.50	972.95	0	10	1
A_8	200.25	501.25	648.50	972.95	0	15	1
A_9	200.25	501.25	648.50	972.95	0	20	1
A_{10}	200.25	501.25	648.50	972.95	0	25	1
A_{11}	200.25	501.25	648.50	972.95	5	5	1
A_{12}	200.25	501.25	648.50	972.95	5	10	1
A_{13}	200.25	501.25	648.50	972.95	5	15	1
A_{14}	200.25	501.25	648.50	972.95	5	20	1
A_{15}	200.25	501.25	648.50	972.95	10	5	1
A_{16}	200.25	501.25	648.50	972.95	10	10	1
A_{17}	200.25	501.25	648.50	972.95	10	15	1
A_{18}	200.25	501.25	648.50	972.95	15	5	1
A_{19}	200.25	501.25	648.50	972.95	15	10	1
A_{20}	200.25	501.25	648.50	972.95	20	5	1

2.3. The Measuring Methods

2.3.1. The Electrical Parameters

The AC electrical resistance of concrete-filled steel tubes was analyzed using a TH2827C precision LCR digital bridge provided by Shenzhen Lexin Intelligent Testing Technology Co., Ltd., Shenzhen, China. The measuring voltage and frequency were 1 V and 10^4 Hz, respectively, corresponding to the sampling frequency of 10 Hz. The Wellington RST5060F Electrochemical Workstation, purchased from Honghua Instrument Equipment Industry and Trade Co., Ltd., Gongyi, China, was used to plot the AC impedance spectrum curves. The frequency settings of the Electrochemical Workstation ranged from 10^5 Hz to 1 Hz with an AC voltage of −10 mV~10 mV. Figure 1 shows the measuring process of ultrasonic and electrical performance parameters.

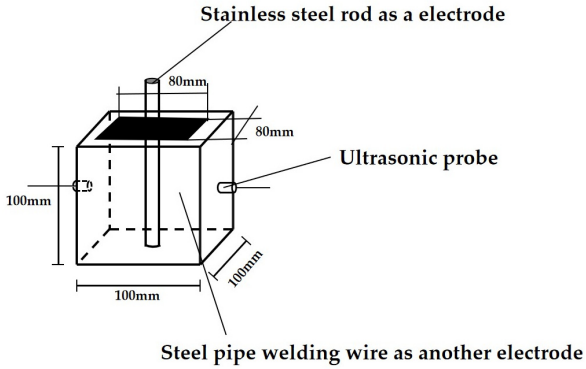

Figure 1. The measuring process of ultrasonic and electrical performance parameters.

2.3.2. The Mass Loss Rate

The mass of the steel tubes was determined before corrosion. After the concrete-filled steel tubes encountered salt erosion, their corroded surfaces were sanded with sandpaper. The steel tubes' mass loss rates (MRs) were calculated to determine the concrete-filled steel tubes' corrosion.

2.3.3. The Micro-Analysis

Steel tube rust samples were collected for analysis using scanning electron microscopy–energy-dispersive spectrometry (SEM-EDS) images and X-ray diffraction (XRD) curves. A Thermofly Axia Chemi SEM tungsten-filament scanning electron microscope (Thermo Fisher Scientific., Shanghai, China) and a wave-sound desktop X-ray diffractometer by Suzhou Langsheng Scientific Instrument Co., Ltd., Suzhou, China, were used for generating the SEM photos and XRD curves.

2.3.4. The Experimental Conditions of NaCl Freeze–Thaw Cycles and Dry–Wet Alternations

The concrete-filled steel tubes were immersed in a NaCl solution with a concentration of 3% for 4 days after 24 days of curing in a standard environment. Then, some specimens were moved to a fully automatic freeze–thaw concrete test box, obtained from Anhui Annai Instrument Co., Ltd., Ma'anshan City, China. The NaCl freeze–thaw cycles (F-C) continued for 300 cycles. The freeze–thaw temperature ranged from −18 °C to 8 °C. During each NaCl dry–wet alternation (D-A), specimens were immersed in the NaCl solution for 8 h; after that, the surfaces of the specimens were dried using a rag. Then, the specimens were dried at a temperature of 80 °C for 36 h. Ultimately, the samples were cooled for 2 h. The Chinese standard GB/T 50082-2009 was used for the measurements of NaCl freeze–thaw cycles and dry–wet alternations [22].

3. Results and Discussion

3.1. The MR of Steel Tubes

The MRs of the steel tubes are shown in Figure 2. As observed in Figure 2, steel tubes' MRs increased after NaCl F-C and NaCl D-A. After using 300 NaCl F-C and 30 NaCl D-A, the MRs were 0%~0.00470% and 0%~0.00666%, respectively. The freeze–thaw cycle of sodium chloride and the alternating dry–wet action caused an increase in cracking and the widening of cracks at the interface between steel pipes and concrete [23,24]. Moreover, the MRs decreased with the added benzotriazole and sodium molybdate because benzotriazole forms an adsorption layer at the interface between the steel pipe and concrete, thereby enhancing the corrosion resistance of the steel pipe and reducing its mass loss [25,26]. Notably, the compactness of the passivation film at the interface between steel pipes and concrete improved with the addition of sodium molybdate, thereby enhancing the corrosion resistance of the steel pipes and reducing their mass loss. When the assembly unit comprised 5 kg/m^3 of sodium molybdate and 15 kg/m^3 of benzotriazole, the mass loss rates of the steel tubes were the lowest. The mass loss of the concrete-filled steel tubes

with benzotriazole was lower than that with sodium molybdate. Moreover, the mass loss of the concrete-filled steel tubes after NaCl dry–wet alternation was higher than that after NaCl freeze–thaw cycles.

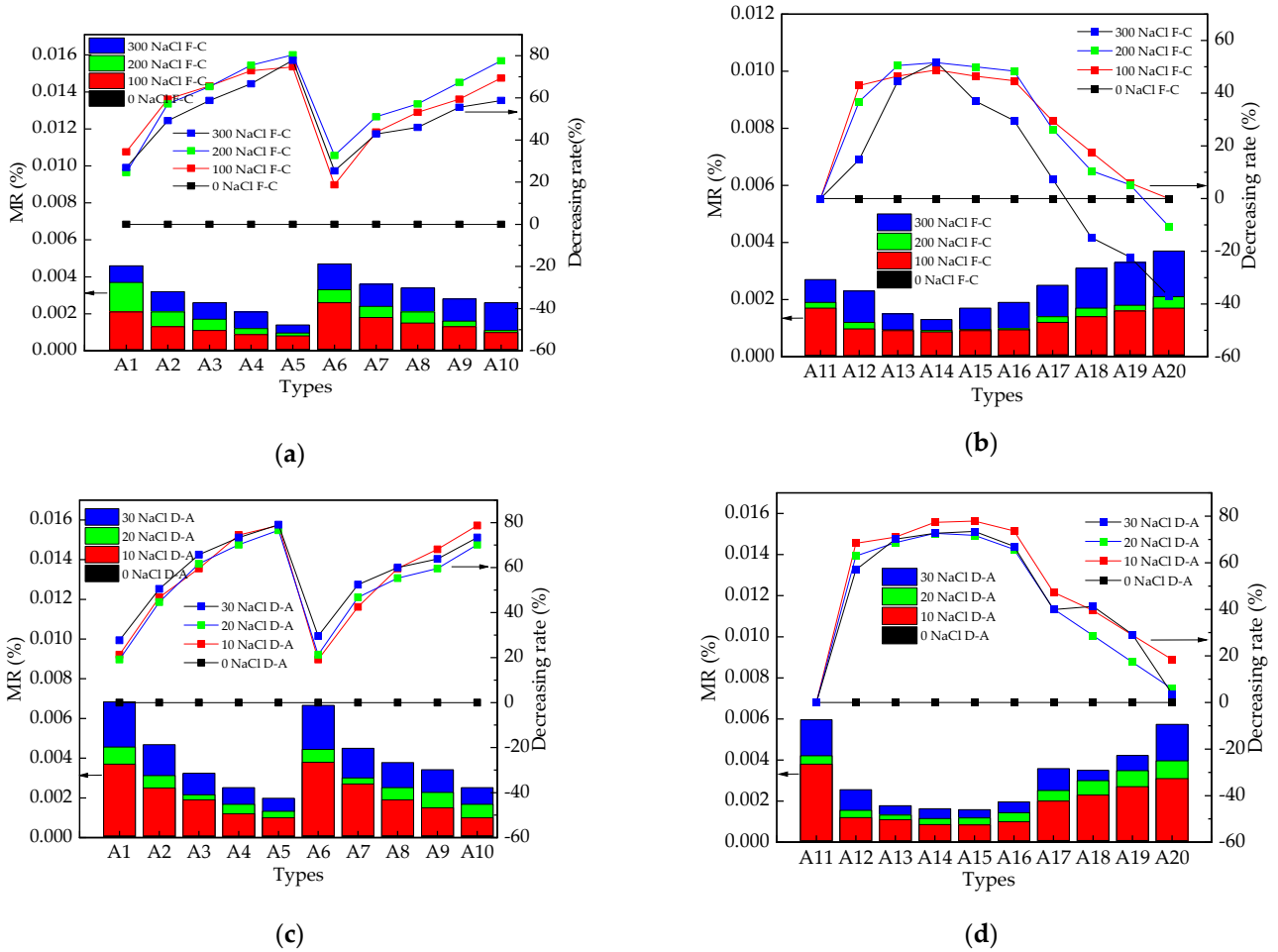

Figure 2. The mass loss rates of steel tubes: (**a**) with a single rust inhibitor, after NaCl F-C; (**b**) with an assembly unit of rust inhibitors, after NaCl F-C; (**c**) with a single rust inhibitor, after NaCl D-A; (**d**) with an assembly unit of blended rust inhibitors, after NaCl D-A.

3.2. The Ultrasonic Velocity of Concrete-Filled Steel Tube

The ultrasonic velocity of the concrete-filled steel tubes is exhibited in Figure 3. The number of NaCl F-C and NaCl D-A had a decreasing effect on the concrete-filled steel tube's ultrasonic velocity. This can be explained by the accelerating action of NaCl F-C and NaCl D-A on the corrosion of steel pipes and alkali–aggregate reaction, thereby exacerbating the development of concrete cracks [27]. Cracks in cement concrete prevent the propagation of ultrasound in concrete, leading to a decrease in ultrasound values. The added corrosion inhibitors can increase the ultrasonic velocity of concrete-filled steel tubes because the inhibitors can prevent the corrosion of steel pipes, thus delaying the cracking of concrete, resulting in a decrease in ultrasonic velocity [28]. An increase in the amount of anticorrosion admixture increased the ultrasonic velocity and the corresponding increasing rate. Concrete-filled steel tubes with benzotriazole had higher ultrasonic velocity than those mixed with Na_2MoO_4. Concrete-filled steel tubes with an assembly unit of anticorrosion admixtures had higher ultrasonic velocity than those with the addition of a single rust inhibitor. The concrete-filled steel tubes with 5 kg/m^3 Na_2MoO_4 and 15 kg/m^3 benzotriazole had the highest ultrasonic velocity and increasing rate. Moreover, the concrete-filled steel tubes had higher ultrasonic velocity after NaCl F-C than after NaCl D-A.

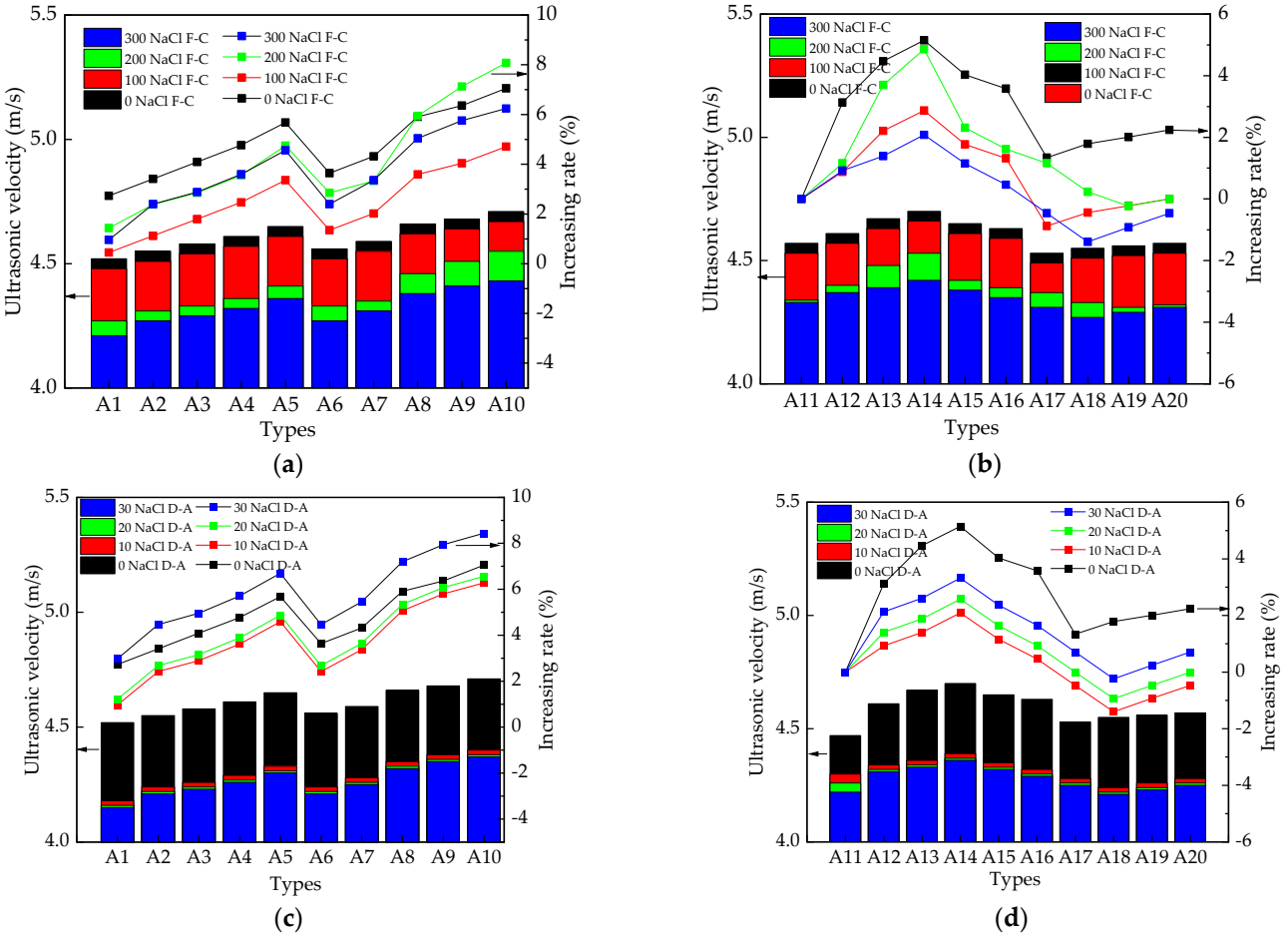

Figure 3. The ultrasonic velocity of concrete-filled steel tube: (**a**) with a single rust inhibitor, after NaCl F-C; (**b**) with an assembly unit of rust inhibitors, after NaCl F-C; (**c**) with a single rust inhibitor, after NaCl D-A; (**d**) with an assembly unit of blended rust inhibitors, after NaCl D-A.

3.3. The Electrical Resistance of Concrete-Filled Steel Tubes

The electrical resistance of concrete-filled steel tubes is illustrated in Figure 4. It can be observed from Figure 4 that before NaCl action, electrical resistance increases with the increasing dosages of benzotriazole and sodium molybdate, as benzotriazole forms an adsorption film at the interface between the steel pipe and concrete in the concrete-filled steel pipes [29]. The adsorption film prevents the migration of electrons in the steel pipe and pore solution ions in the concrete, resulting in a decrease in the conductivity of the concrete-filled steel pipes. Sodium molybdate makes the passivation film more dense, causing a decrease in electron and ion migration and an increase in electrical resistance. The concrete-filled steel tube with 5 kg/m^3 Na_2MoO_4 and 15 kg/m^3 benzotriazole had the highest electrical resistance. An increase in the number of NaCl F-C and NaCl D-A led to an increase in the electrical resistance of the concrete-filled steel tubes. This is due to the increased rust on the surface of the steel tube induced by the NaCl action, which blocks the migration of electrons and free ions. With the increase in the number of NaCl F-C and NaCl D-A actions, the electrical resistance of the concrete-filled steel tubes decreased with the addition of benzotriazole and sodium molybdate. This is because benzotriazole and sodium molybdate can improve the rust resistance of steel pipes, thereby reducing the rust stains on the steel. As the rust on steel reduced its electrical conductivity, the decrease in the electrical conductivity of concrete-filled steel pipes slowed down [30,31]. Thus, the electrical resistance of the concrete-filled steel tubes after undergoing the NaCl action decreased by adding benzotriazole and sodium molybdate.

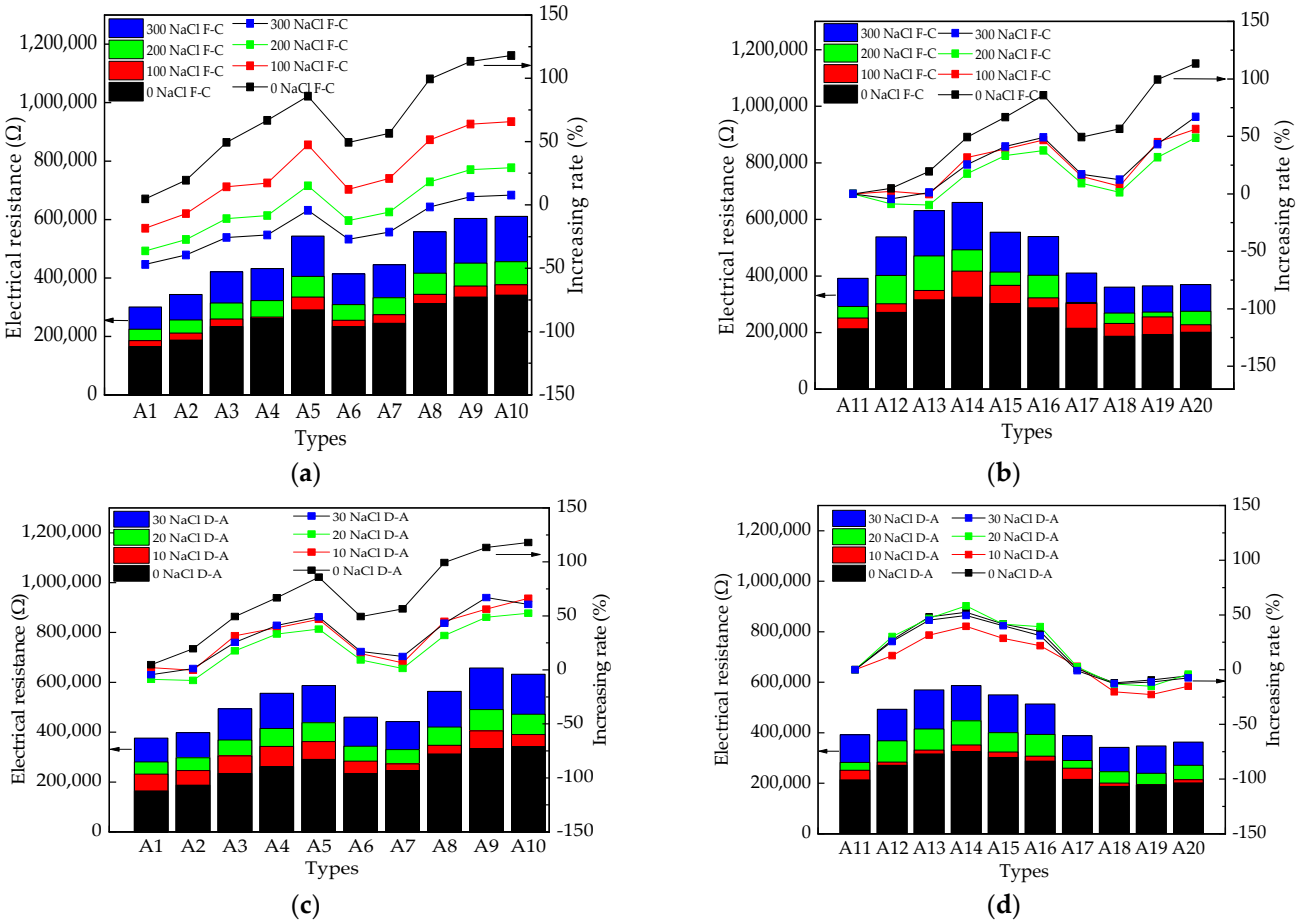

Figure 4. The electrical resistance of steel tubes: (**a**) with a single rust inhibitor, after NaCl F-C; (**b**) with assembly unit of rust inhibitor, after NaCl F-C; (**c**) with a single rust inhibitor, after NaCl D-A; (**d**) with assembly unit of rust inhibitors, after NaCl D-A.

3.4. The AC Impedance Spectrum Curves of Concrete-Filled Steel Tubes

Figure 5 depicts the AC impedance spectrum curves of the concrete-filled steel tubes. In Figure 5, Z_r values represent the actual electrical resistance values in the AC impedance spectra, while Z_i values represent the electrical reactance values. The interface between the steel pipe and concrete, the interface between aggregate and cement mortar, and the interface between the liquid phase and solid phase of the pore solution are the mechanisms involved in concrete-filled steel pipes [23]. Therefore, the capacitance value in concrete-filled steel pipes is relatively high. The maximum values of electrical resistance increased with the increase in the number of NaCl F-C and NaCl D-A actions since the NaCl action can accelerate the corrosion of steel pipes and the cracking of concrete, hindering the propagation of the charged particle [32]. Consequently, Z_r increased by the NaCl action. After the NaCl action, Z_r decreased by adding the rust inhibitor owing to the fact that the rust inhibitors delayed the corrosion of steel pipes, thereby reducing the increasing rate of the electrical resistance of concrete-filled steel pipes after the NaCl action [33]. The concrete-filled steel tubes with the assembly unit of 5 kg/m^3 Na_2MoO_4 and 15 kg/m^3 benzotriazole had the highest Z_r corresponding to the peaks observed in AC impedance spectrum curves.

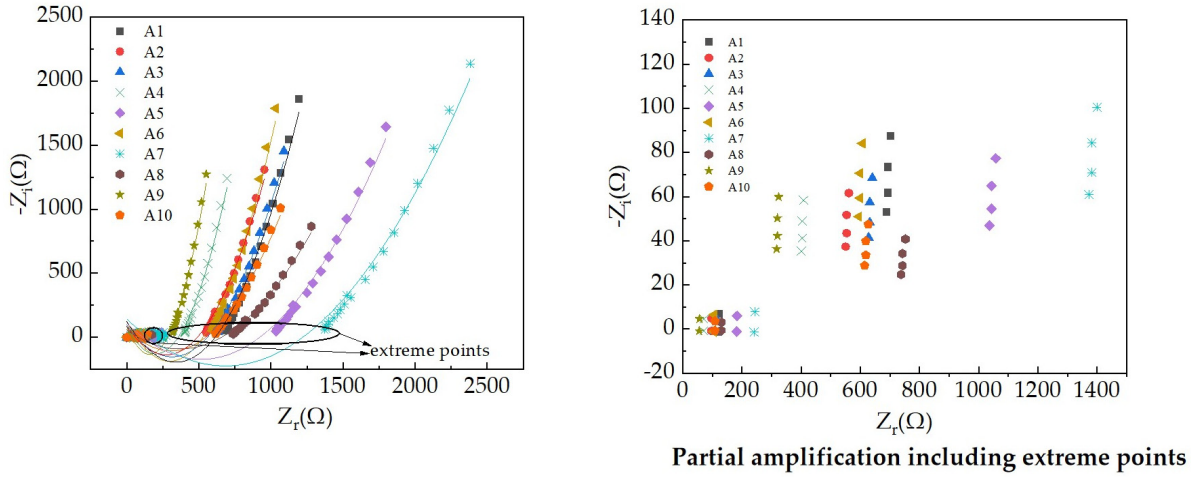

(**a**)

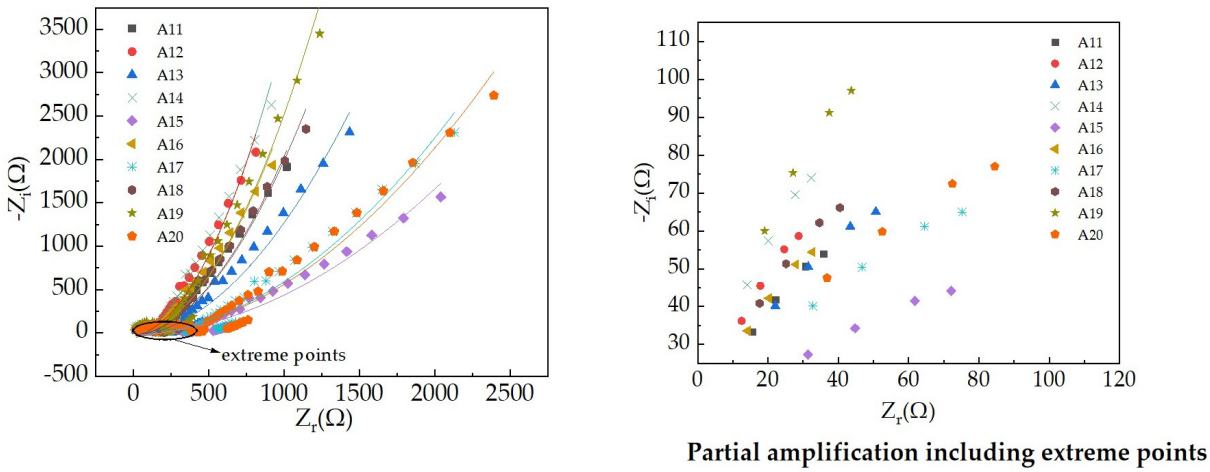

(**b**)

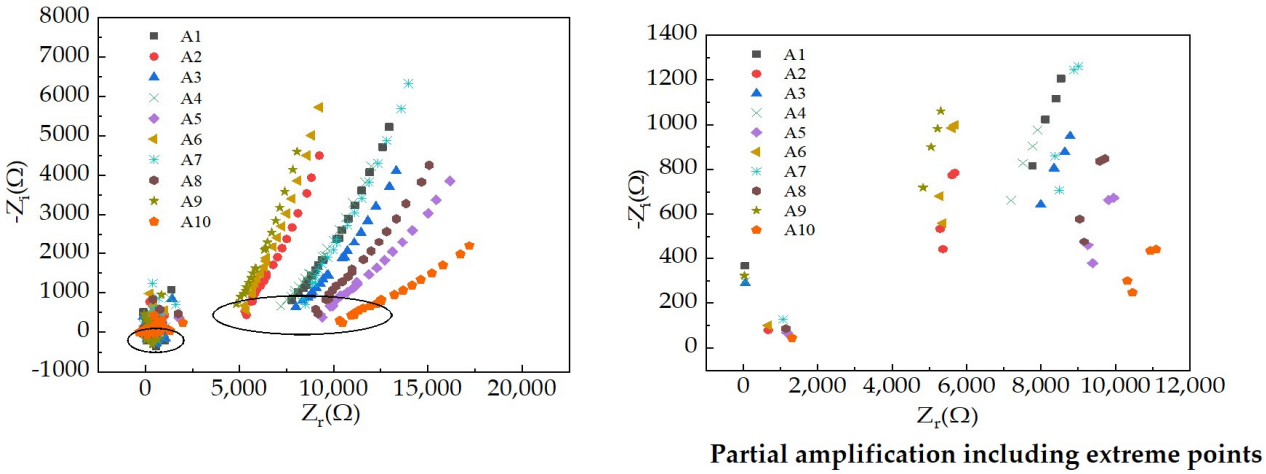

(**c**)

Figure 5. *Cont.*

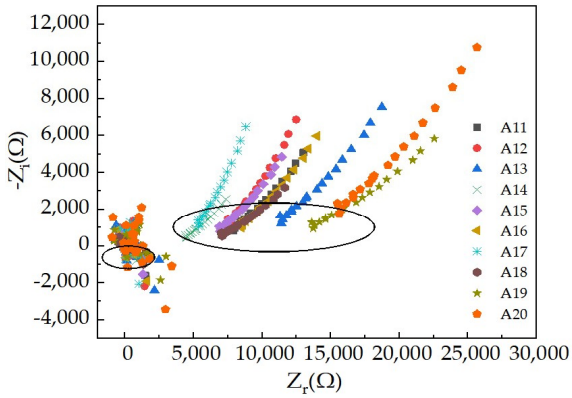

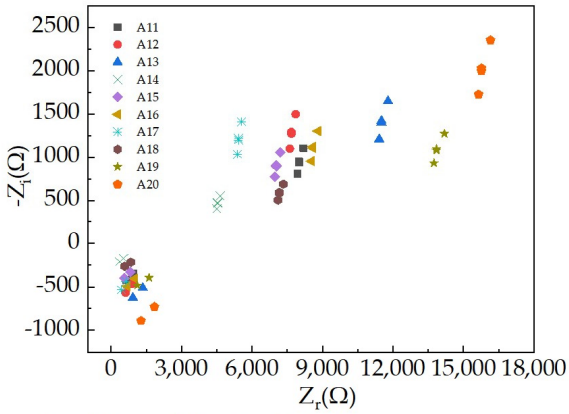

Partial amplification including extreme points

(**d**)

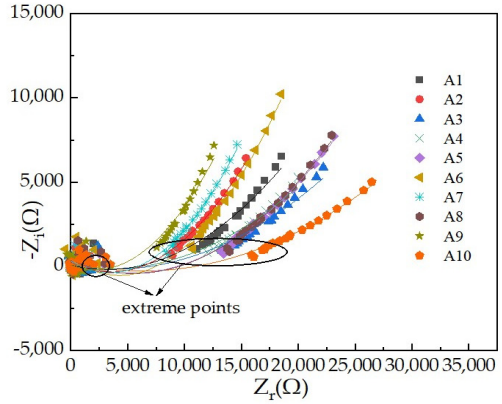

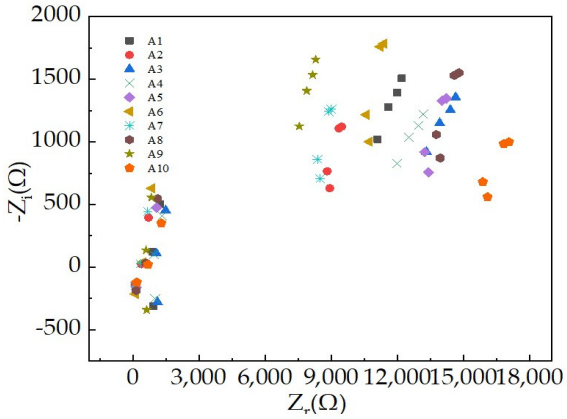

Partial amplification including extreme points

(**e**)

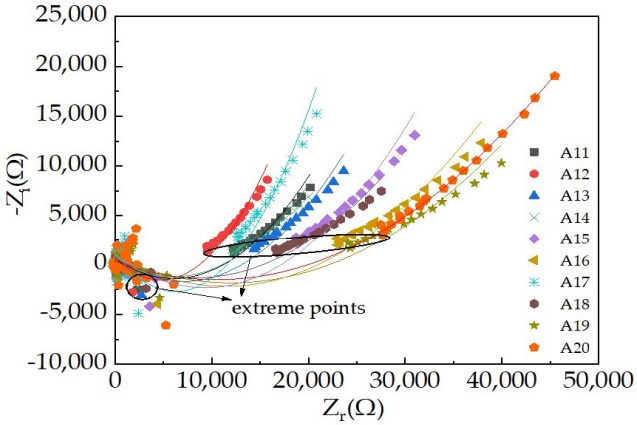

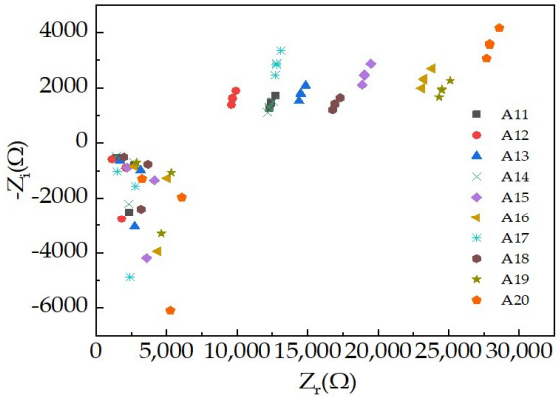

Partial amplification including extreme points

(**f**)

Figure 5. The AC impedance spectrum curves of concrete-filled steel tubes: (**a**) with a single rust inhibitor, before salt erosion; (**b**) with assembly unit of rust inhibitor, before salt erosion; (**c**) with a single rust inhibitor, after NaCl F-C; (**d**) with assembly unit of rust inhibitor, after NaCl F-C; (**e**) with a single rust inhibitor, after NaCl D-A; (**f**) with assembly unit of rust inhibitors, after NaCl D-A.

The impedance spectrum fitting software ZSimpWin, version 3.5, was used for obtaining the equivalent circuits of the AC impedance spectrum curves. The detailed process can be found in a previous study [34]. The equivalent circuits of the AC impedance spectrum curves are depicted in Figure 6. It is observed that the equivalent circuits are composed of four electrical components. One of the four electrical components was the contact electrical resistance (the electrical resistance between the steel pipes and concrete). The other three electrical components were the parallel electrical resistances and capacitances of the rust, the pore solution, and the concrete matrix. The Chi values of the equivalent circuits were all lower than 0.034, indicating the accuracy of the equivalent circuits.

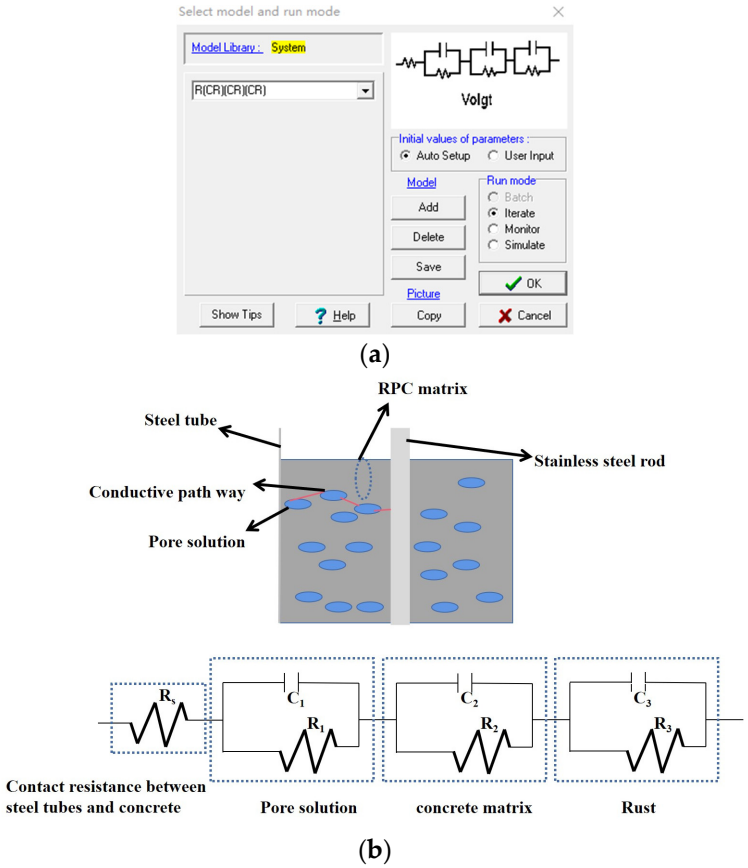

Figure 6. The equivalent circuits of concrete-filled steel tubes: (**a**) the equivalent circuits in impedance spectrum fitting software ZSimpWin; (**b**) detailed images of the equivalent circuits.

The electrical resistance of the rust on the surface of the steel pipes is displayed in Figure 7. The electrical resistance of the rust showed an increasing trend with the increase in the number of NaCl F-C and NaCl D-A, due to the increase in the rust area on the surface of the steel tube, which hindered the migration of electrons and increased the electrical resistance. However, an increase in the dosages of the rust inhibitors had a decreasing effect on the rust's electrical resistance. The reducing effect of benzotriazole on the rust's electrical resistance was higher than that of Na_2MoO_4. The reducing effect of an assembly unit comprising 5 kg/m^3 of Na_2MoO_4 and 15 kg/m^3 of benzotriazole on the rust's electrical resistance was the highest. The rust's electrical resistance after 30 NaCl D-A was higher than that after 300 NaCl F-C.

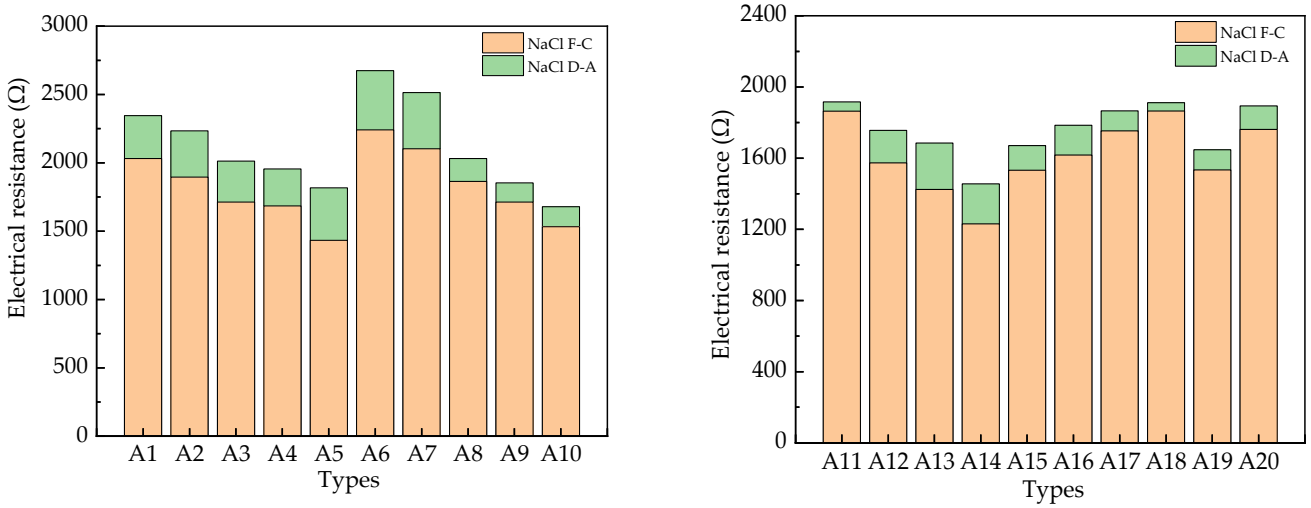

Figure 7. The electrical resistance of concrete-filled steel tubes: (**a**) with a single rust inhibitor; (**b**) with an assembly unit of rust inhibitors.

3.5. The Tafel Curves of Concrete-Filled Steel Tubes

Figure 8 displays the Tafel curves of concrete-filled steel tubes after 300 NaCl F-C and 30 NaCl D-A. As can be seen, the Tafel curves are divided into two parts. In the first part, the potential is almost unchanged with the increasing log (current). In the second part, the curves are divided into two sections; in the first section, the potential increases with the increasing log (current). However, in the second section, the potential decreases with the increasing log (current). Equation (1) is used to calculate the corrosion area rate of steel pipes [30]. In Equation (1), v represents the steel tube's corrosion rate, with the unit expressed as g/m^2h; m is the metal's atomic weight, with the unit of g; i stands for the corrosion current density, and its unit is $\mu A/cm^2$. The key parameters (AC impedance spectrum curves' actual values corresponding to the maximum points and corrosion current densities in the Tafel curves) characterizing the corrosion of steel pipes are shown in Tables A1 and A2 (in Appendix A), respectively.

$$v = \frac{10m}{\frac{9.65\times10^4}{3.6}N}i = 3.73\times10^{-4}\frac{m}{N}i \quad (1)$$

Figure 9 demonstrates the corrosion area rate of the concrete-filled steel tubes calculated with Equation (1). As shown in Figure 9, the corrosion area rate exhibited an increasing trend with the increase in the number of NaCl F-C and NaCl D-A. This can be explained by the effect of NaCl action on the accelerated corrosion of steel pipes [35]. In terms of the corrosion inhibitors, the corrosion area rate of steel pipes decreased with an increase in corrosion inhibitors' dosages. As mentioned in the previous section, the decrease in the corrosion area rate is mainly due to the improved rust resistance performance of the rust inhibitors [21,36]. The concrete-filled steel tube with the assembly unit of 5 kg/m^3 Na_2MoO_4 and 15 kg/m^3 benzotriazole had the lowest corrosion area rate. The corrosion area rate of the concrete-filled steel tube with benzotriazole was lower than that with Na_2MoO_4. Additionally, the corrosion area rate of the concrete-filled steel tube after 30 NaCl D-A was higher than that after 300 NaCl F-C.

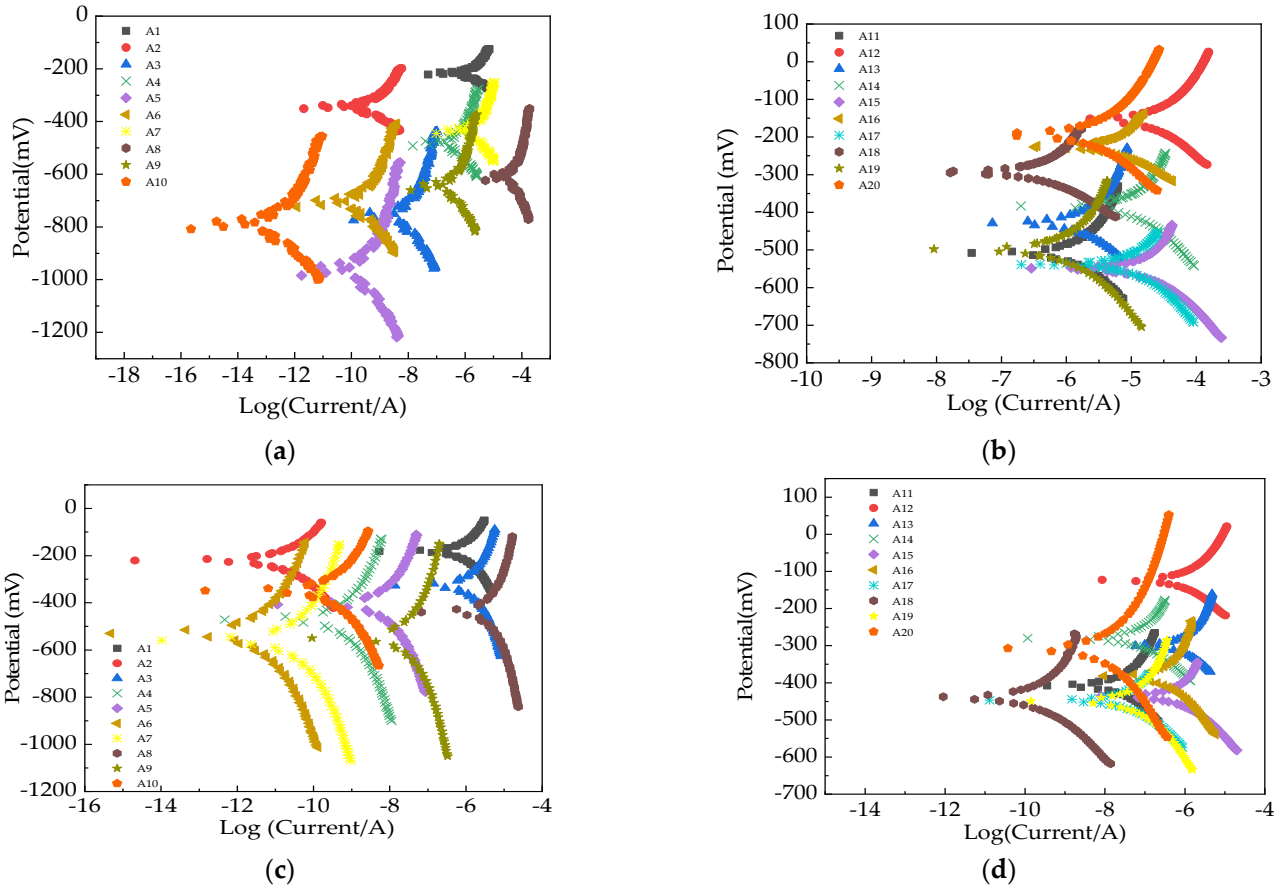

Figure 8. The AC impedance spectrum curves of concrete-filled steel tubes: (**a**) with a single rust inhibitor, after NaCl F-C; (**b**) with assembly unit of rust inhibitor, after NaCl F-C; (**c**) with a single rust inhibitor, after NaCl D-A; (**d**) with an assembly unit of rust inhibitors, after NaCl D-A.

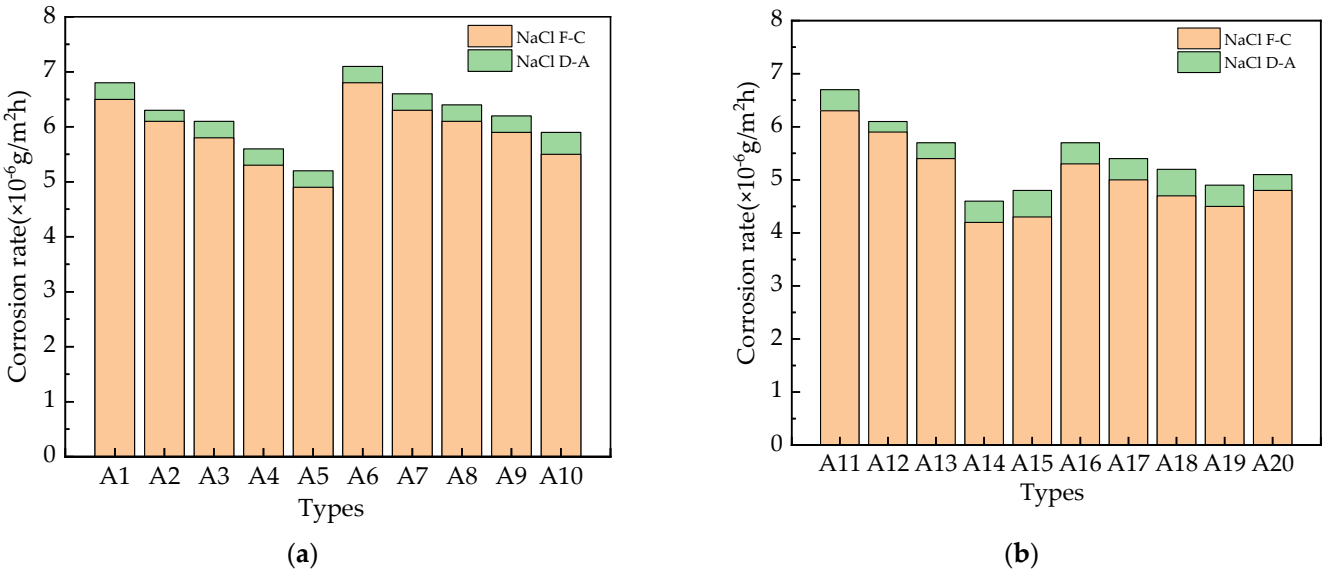

Figure 9. The corrosion rate of concrete-filled steel tubes: (**a**) with a single rust inhibitor; (**b**) with an assembly unit of rust inhibitors.

3.6. The EDS of the Rust

The SEM-EDS results of the rust on the surface of the steel tubes are displayed in Figure 10. Figure 10a shows the micrographs (magnified by 100 times) of the rust samples used for SEM-EDS experiments. The testing zones of SEM-EDS are labeled in Figure 10a. It was found that the rust on the surface of the steel tubes consisted of Fe, Cl, Ca, C, O, Na, Ni, and Si. The A10 concrete-filled steel tubes after 300 NaCl F-C and 30 NaCl D-A were selected. As shown in Figure 10, the Fe content after 30 NaCl D-A was higher than that after 300 NaCl F-C due to the fact that the steel tubes corroded more seriously after NaCl D-A. Therefore, the Fe content was the highest after 30 NaCl D-A. Moreover, the Fe concentration of the rust on the surface of the concrete-filled steel tube with the assembly unit of 5 kg/m^3 Na_2MoO_4 and 15 kg/m^3 benzotriazole was the lowest, which was attributed to its best corrosion resistance.

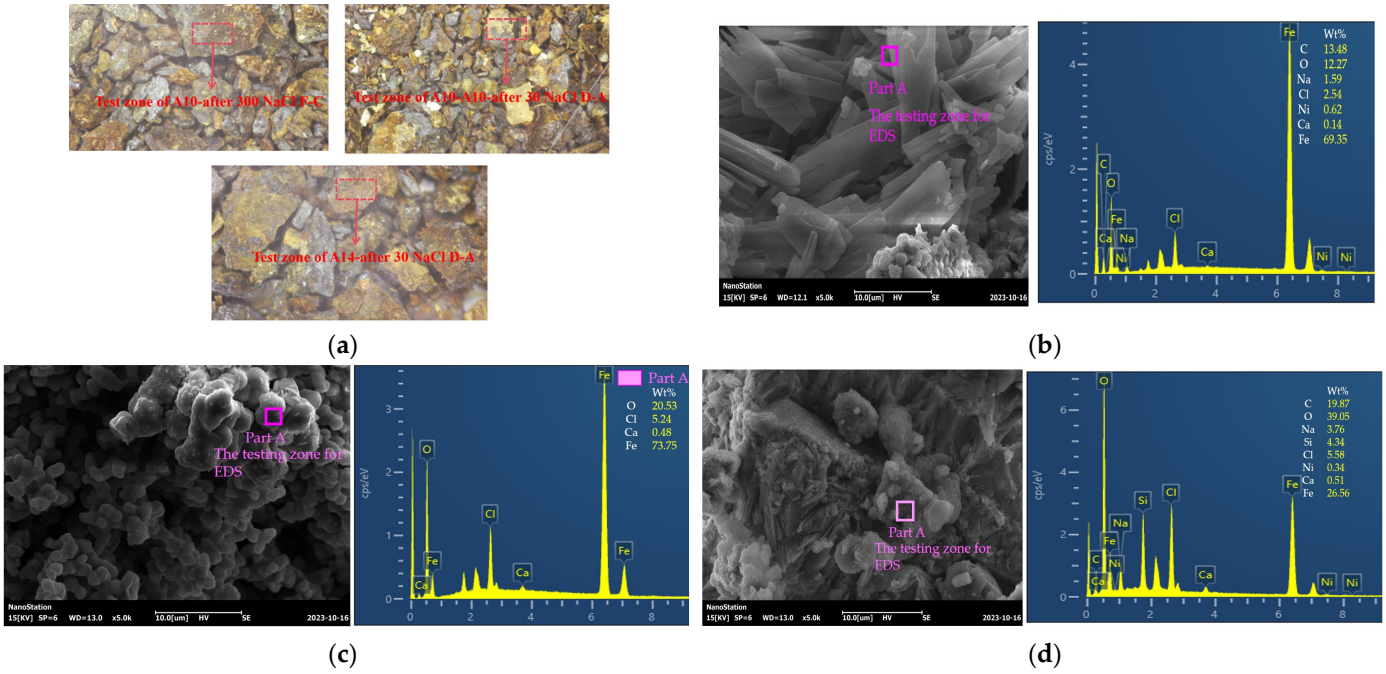

Figure 10. The SEM-EDS of rust on the surface of the steel tubes: (**a**) micrographs of samples; (**b**) A10, after 300 NaCl F-C; (**c**) A10, after 30 NaCl D-A; (**d**) A14, after 30 NaCl D-A.

3.7. The XRD Curves of the Rust

The XRD curves of the rust on the surface of the steel tubes are exhibited in Figure 11. The rust consisted of α-FeO(OH), β-FeO(OH), Fe_2O_3, and Fe_3O_4. A higher number of Fe_2O_3 and Fe_3O_4 crystals were observed after 30 NaCl D-A than after 300 NaCl F-C. NaCl F-C and NaCl D-A can accelerate the rate at which chloride ions damage the passivation film on the surface of the steel, thereby accelerating the corrosion of iron, resulting in the formation of crystals such as α-FeO(OH), β-FeO(OH), Fe_2O_3, and Fe_3O_4. The corrosion effect of 30 NaCl D-A on the passivation film was more serious than that of 300 NaCl F-C. The Fe_2O_3 and Fe_3O_4 concentrations in the specimens with the assembly unit of 5 kg/m^3 Na_2MoO_4 and 15 kg/m^3 benzotriazole were the lowest.

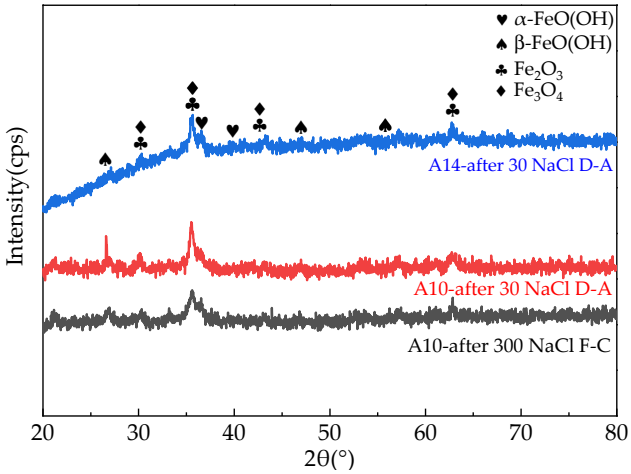

Figure 11. The XRD curves of rust on the surface of the steel tube.

4. Conclusions

The effect of an assembly unit of Na_2MoO_4 and benzotriazole on the corrosion resistance of concrete-filled steel tubes was investigated. The following conclusions can be drawn:

The MRs increased at the rates of 0%~0.00470% and 0%~0.00666% after 300 NaCl F-C and 30 NaCl D-A. Moreover, the corresponding ultrasonic velocities were 0%~21.1% and 0%~23.6%. When the rust inhibitor was added, the results were the opposite. The addition of Na_2MoO_4 and benzotriazole decreases the MRs at the rates of 0%~80.3% and 0%~81.6%.

The corresponding ultrasonic velocities were 0%~8.1% and 0%~8.3% after NaCl action. The added rust inhibitors slowed down the reduction in ultrasound speed.

The initial electrical resistance of concrete-filled steel tubes decreased by adding the rust inhibitors with increasing rates of 0%~123% and 0%~127%. Specimens with the assembly unit of cathodic and anodic rust inhibitors had the highest initial electrical resistance.

The increasing rates of electrical resistance after NaCl F-C and NaCl D-A were 81.6% and 87.3%, respectively. The electrical resistance after the specimens were subjected to NaCl F-C and NaCl D-A actions decreased by the decreasing rates of 31.6% and 35.7%, respectively, with Na_2MoO_4 and benzotriazole used as rust inhibitors. Concrete-filled steel tubes with the assembly unit of 5 kg/m^3 Na_2MoO_4 and 15 kg/m^3 benzotriazole had the highest electrical resistance before the NaCl action and the lowest increasing rates by NaCl action.

Before the NaCl action, the resistance values corresponding to the peaks of the AC impedance spectrum curves increased with the addition of rust inhibitors. The NaCl F-C and NaCl D-A actions had an increasing effect on the resistance values corresponding to the peaks of the AC impedance spectrum curves. The equivalent circuits were composed of four electrical components connected in series. The four electrical components were the contact resistances between the steel pipes, stainless steel bars, and cement concrete, as well as the parallel electrical resistances and capacitances of the pore solution, rust, and the concrete matrix. The electrical resistance of the rust decreased by the increase in the dosages of rust inhibitors and increased by the NaCl actions. The concrete-filled steel tubes with 5 kg/m^3 Na_2MoO_4 and 15 kg/m^3 benzotriazole had the highest electrical resistance associated with the peaks before the NaCl action and the lowest increasing rates of electrical resistance. The rust's electrical resistance in the concrete-filled steel tubes with the assembly unit composed of 5 kg/m^3 Na_2MoO_4 and 15 kg/m^3 benzotriazole was the lowest.

The corrosion area rates of the steel pipes increased with NaCl F-C and NaCl D-A. The addition of the rust inhibitors led to a decrease in the corrosion area rates of the steel pipes. The concrete-filled steel tubes with the assembly unit of 5 kg/m^3 Na_2MoO_4 and 15 kg/m^3 benzotriazole had the lowest corrosion area rate.

The rust had the highest Fe concentration after the NaCl D-A action. The rust inhibitors decreased the Fe content. Concrete-filled steel tubes with the assembly unit using 5 kg/m^3 Na_2MoO_4 and 15 kg/m^3 benzotriazole had the lowest concentration of Fe elements and iron oxide crystals.

Author Contributions: Methodology, Z.X. and N.X.; Validation, D.W.; Formal analysis, D.W., Z.X., N.X. and H.W.; Investigation, D.W., Z.X., N.X. and Z.H.; Resources, D.W. and H.W.; Data curation, Z.X., Z.H. and F.S.; Writing—original draft, D.W.; Writing—review & editing, H.W.; Project administration, H.W. and F.S.; Funding acquisition, H.W. All authors have read and agreed to the published version of the manuscript.

Funding: This research was funded by Zhejiang Provincial Natural Science Foundation, grant number LY22E080005, and the research on key technologies for the preparation and assembly of solid waste recycled self-insulating wallboards, grant number 2023JH2/101700001, and the research on new welding technology and life extension strategy of large flange shaft, grant number 2023JH2/101700002.

Institutional Review Board Statement: Not applicable.

Informed Consent Statement: Not applicable.

Data Availability Statement: Data are contained within the article.

Conflicts of Interest: The authors declare no conflict of interest.

Appendix A

Table A1. The maximum points of Zr (Ω) obtained from AC impedance spectrum curves of UHPC before salt erosion.

Types	Maximum Points of Zr (Ω)
A1	688.6
A2	550.2
A3	627.9
A4	400.6
A5	1036.7
A6	594.9
A7	1372.6
A8	737.6
A9	317.6
A10	614.5
A11	183.0
A12	146.2
A13	258.1
A14	164.7
A15	367.4
A16	166.2
A17	383.5
A18	206.1
A19	222.6
A20	430.6

Table A2. The maximum points of Zr (Ω) obtained from AC impedance spectrum curves of UHPC after NaCl F-C.

Types	Maximum Points of Zr (Ω)
A1	7770.0
A2	5364.0
A3	7992.0
A4	7192.8
A5	9387.0
A6	5364.0
A7	8493.0
A8	9162.8
A9	4830.7
A10	10,459.8
A11	7933.5
A12	7611.4
A13	11,417.1
A14	4497.5
A15	6973.8
A16	8527.0
A17	5378.8
A18	7108.4
A19	13,742.7
A20	15,643.3

Table A3. The maximum points of Zr (Ω) obtained from AC impedance spectrum curves of UHPC after NaCl D-A.

Types	Maximum Points of Zr (Ω)
A1	11,100.0
A2	8940.0
A3	13,320.0
A4	11,988.0
A5	13,410.0
A6	10,728.0
A7	8493.0
A8	13,946.4
A9	7548.0
A10	16,092.0
A11	12,300.0
A12	9594.0
A13	14,391.0
A14	12,169.0
A15	18,869.3
A16	23,071.9
A17	12,692.9
A18	16,774.4
A19	24,322.5
A20	27,686.3

Table A4. The corrosion current obtained from Tafel curves of UHPC after NaCl F-C.

Types	Corrosion Current (μA)
A1	0.1
A2	0.1
A3	0.2
A4	0.2
A5	0.2
A6	0.2
A7	0.2
A8	0.3
A9	0.3
A10	0.3
A11	0.1
A12	0.1
A13	0.1
A14	0.1
A15	0.2
A16	0.2
A17	0.2
A18	0.2
A19	0.3
A20	0.3

Table A5. The corrosion current obtained from Tafel curves of UHPC after NaCl D-A.

Types	Corrosion Current (mA)
A1	0.1
A2	0.2
A3	0.2
A4	0.2
A5	0.2
A6	0.3
A7	0.3
A8	0.3
A9	0.3
A10	0.3
A11	0.2
A12	0.2
A13	0.2
A14	0.1
A15	0.3
A16	0.3
A17	0.3
A18	0.3
A19	0.3
A20	0.3

References

1. Yang, J.; Huang, J.; Su, Y.; He, X.; Tan, H.; Yang, W.; Strnadel, B. Eco-friendly treatment of low-calcium coal fly ash for high pozzolanic reactivity: A step towards waste utilization in sustainable building material. *J. Clean. Prod.* **2019**, *238*, 117962. [CrossRef]
2. Yokota, H.; Kato, E.; Iwanami, M. Chloride-induced corrosion of reinforcement and its effect on performance of structures. *Int. J. Model. Identif. Control* **2009**, *7*, 179–184. [CrossRef]
3. Abrishambaf, A.; Pimentel, M.; Nunes, S. Influence of fiber orientation on the tensile behavior of ultra-high performance fiber reinforced cementitious composites. *Cem. Concr. Res.* **2017**, *97*, 28–40. [CrossRef]
4. Zhang, P.; Cong, Y.; Vogel, M.; Liu, Z.; Müller, H.S.; Zhu, Y.; Zhao, T. Steel reinforcement corrosion in concrete under combined actions: The role of freeze-thaw cycles, chloride ingress, and surface impregnation. *Constr. Build. Mater.* **2017**, *148*, 113–121. [CrossRef]

5. Zhang, P.; Wang, C.; Gao, Z.; Wang, F. A review on fracture properties of steel fiber reinforced concrete. *J. Build. Eng.* **2023**, *67*, 105975. [CrossRef]
6. Luo, X. Mechanical properties of steel fiber reinforced concrete material in construction of road bridge deck. *Bridge Struct.* **2021**, *16*, 169–176. [CrossRef]
7. Kumar, S.; Kumar Gupta, P.; Iqbal, M.A. Experimental and numerical study on self-compacting alkali-activated slag concrete-filled steel tubes. *J. Constr. Steel Res.* **2024**, *214*, 108453. [CrossRef]
8. Liu, W.; Wang, X.; Guo, Y.; Tian, Z.; Li, J.; Bai, W. Experimental and numerical study of L-shaped irregularly concrete-filled steel tube columns under axial compression and eccentric compression. *J. Build. Eng.* **2024**, *84*, 108572. [CrossRef]
9. Zhou, X.; Hou, D.; Chen, T.; Wang, X. The development of concrete filled steel tube with enhanced performance via the use of expansive ultra high performance concrete. *J. Build. Eng.* **2023**, *79*, 107793. [CrossRef]
10. Song, S.; Chen, J.; Ye, J.; Quan, G.; Wang, Z.; Xiao, J. Test and analysis of the interfacial bond behaviour of circular concrete-filled wire-arc additively manufactured steel tubes. *J. Build. Eng.* **2024**, *82*, 108171. [CrossRef]
11. Wei, B.; Wei, Y.; Lin, Y.; Wang, G.; Zhang, Y. Compressive performance of bamboo scrimber and concrete-filled steel tube columns. *Eng. Struct.* **2024**, *300*, 117192. [CrossRef]
12. Dai, P.; Yang, L.; Wang, J.; Lin, M.; Fan, J. Bond stress-slip relationship in concrete-filled square stainless steel tubes. *Constr. Build. Mater.* **2022**, *326*, 127001. [CrossRef]
13. Zhong, Y.; Zhao, O.; Young, B. Experimental and numerical investigations of recycled aggregate concrete-filled stainless steel tube stub columns under combined compression and bending. *Eng. Struct.* **2022**, *266*, 114502. [CrossRef]
14. Yu, M.; Liao, W.; Liu, S.; Wang, T.; Yu, C.; Cheng, S. Axial compressive performance of ultra-high performance concrete-filled steel tube stub columns at different concrete age. *Structures* **2023**, *55*, 664–676. [CrossRef]
15. George, C.; Senthil Selvan, S.; Sathish Kumar, V.; Murali, G.; Giri, J.; Makki, E.; Sathish, T. Enhancing the fire-resistant performance of concrete-filled steel tube columns with steel fiber-reinforced concrete. *Case Stud. Constr. Mater.* **2024**, *20*, e02741. [CrossRef]
16. Ma, H.; Liu, F.; Fang, L.; Zhao, Y.; Gan, X. Cyclic loading tests and seismic behaviors of steel-reinforced recycled aggregate concrete filled square steel tube composite columns. *J. Constr. Steel Res.* **2024**, *212*, 108270. [CrossRef]
17. Jiang, H.; Ye, Y.; Lai, S. Behavior of seawater sea sand concrete-filled plastic-lined steel tube stub columns under axial compression. *Structures* **2023**, *58*, 105577. [CrossRef]
18. Yan, Y.; Lu, Y.; Li, S.; Wu, Z. Square concrete-filled steel tube strengthened with carbon fiber-reinforced polymer grid-reinforced engineered cementitious composite under axial loading. *Eng. Struct.* **2024**, *299*, 117108. [CrossRef]
19. Lu, L.; Zhang, T.; Liang, T.; Ren, Q. Axial compressive behavior of circular concrete-filled steel tube stub columns with steel slag coarse aggregate. *Structures* **2023**, *51*, 1893–1905. [CrossRef]
20. Bahrami, A.; Nematzadeh, M. Bond behavior of lightweight concrete-filled steel tubes containing rock wool waste after exposure to high temperatures. *Constr. Build. Mater.* **2021**, *300*, 124039. [CrossRef]
21. Bharath, B.R.; Shweta, H.J.; Akib, J.; Golden, K. Mechanical and corrosion behavior of sheet-based 316L TPMS structures. *Int. J. Mech. Sci.* **2023**, *254*, 108439.
22. *GB/T 50082-2009*; Standard for Test Method of Long-Term Performance and Durability of Ordinary Concrete. China Standard Press: Beijing, China, 2009.
23. Zhu, J.; Liu, S.; Song, L.; Qu, Z.; Wang, H. Influence of Carbon Dioxide Curing on the Corrosion Resistance of Reinforced Cement Mortar under the External Erosion of NaCl Freeze–Thaw Cycle. *Appl. Sci.* **2022**, *12*, 5061. [CrossRef]
24. Wang, H.; Jin, K.; Zhang, A.; Zhang, L.; Han, Y.; Liu, J.; Shi, F.; Feng, L. External erosion of sodium chloride on the degradation of self-sensing and mechanical properties of aligned stainless steel fiber reinforced reactive powder concrete. *Constr. Build. Mater.* **2021**, *287*, 123028. [CrossRef]
25. Liu, Q.; Zhang, Z.; Zhang, S.G.; Li, X.L.; Long, H.C.; Meng, X.X.; Melnikov, A.L. The influence of particle morphology on the long-term strength of sandy soil under freeze-thaw cycles. *Case. Stud. Constr. Mater.* **2023**, *18*, e02196. [CrossRef]
26. Jiang, H.; Wang, W.; Wang, H. The Corrosion Resistance of Reinforced Reactive Powder Concrete with Secondary Aluminum Ash Exposed to NaCl Action. *Materials* **2023**, *16*, 5615. [CrossRef] [PubMed]
27. Wang, H.; Gao, X.; Liu, J. Coupling effect of salt freeze-thaw cycles and cyclic loading on performance degradation of carbon nanofiber mortar. *Cold Reg. Sci. Technol.* **2018**, *154*, 95–102. [CrossRef]
28. Wang, H.; Gao, X.; Liu, J. Effects of salt freeze-thaw cycles and cyclic loading on the piezoresistive properties of carbon nanofibers mortar. *Constr. Build. Mater.* **2018**, *115*, 126–133. [CrossRef]
29. Nam, N.; Hien, P.; Hoai, N.; Thu, V. A study on the mixed corrosion inhibitor with a dominant cathodic inhibitor for mild steel in aqueous chloride solution. *J. Taiwan Inst. Chem. Eng.* **2018**, *91*, 556–569. [CrossRef]
30. Wang, H.; Zhang, A.; Zhang, L.; Liu, J.; Han, Y.; Shu, H.; Wang, J. Study on the influence of compound rust inhibitor on corrosion of steel bars in chloride concrete by electrical parameters. *Constr. Build. Mater.* **2020**, *262*, 120763. [CrossRef]
31. Tang, Z. A review of corrosion inhibitors for rust preventative fluids. *Curr. Opin. Solid State Mater. Sci.* **2019**, *23*, 100759. [CrossRef]
32. Alhozaimy, A.; Hussain, R.R.; Al-Negheimish, A. Electro-chemical investigation for the effect of rebar source and surface condition on the corrosion rate of reinforced concrete structures under varying corrosive environments. *Constr. Build. Mater.* **2020**, *244*, 118317. [CrossRef]
33. Ben Mansour, H.; Dhouibi, L.; Idrissi, H. Effffect of phosphate-based inhibitor on prestressing tendons corrosion in simulated concrete pore solution contaminated by chloride ions. *Constr. Build. Mater.* **2018**, *171*, 250–260. [CrossRef]

34. Chung, D.D.L.; Xi, X. A review of cement-based materials as electroceramics. *Ceram. Int.* **2023**, *49*, 24621–24642. [CrossRef]
35. Kumar Tiwari, A.; Purnima, S.; Goyal, V. Influence of corrosion inhibitors on two different concrete systems under combined chloride and carbonated environment. *Structures* **2023**, *48*, 717–735. [CrossRef]
36. Chen, T.; Zhang, X.; Wang, J. Investigation on Effect of Different Inhibitors on Corrosion Behavior of 45# Steel in Simulated Concrete Pore Solution. *Int. J. Electrochem. Sci.* **2022**, *17*, 221283.